Coherent Swing Instability of Interconnected Power Grids and a Mechanism of Cascading Failure

Yoshihiko Susuki, Igor Mezić, and Takashi Hikihara

Abstract We describe a dynamical mechanism of cascading failure in a system of interconnected power grids. This mechanism is based on the discovery of (Susuki Y et al. (2011) J Nonlinear Sci 21(3):403–439), an emergent and undesirable phenomenon of synchronous machines in a power grid, termed the Coherent Swing Instability (CSI). In this phenomenon, most of the machines in a sub-grid coherently lose synchronism with the rest of the grid after being subjected to a local and finite disturbance. By numerical analysis of a system of weakly interconnected power grids, we present a phenomenon of coupled swing dynamics in which the CSI happens for all of the power grids in a successive manner. We suggest that a small disturbance in one grid can grow, spill to the other grids, and cause the whole system to fail. This mechanism enables the development of dynamically relevant tools for monitoring and control of wide-area disturbances, which become feasible when the physical power network is overlaid with an information network, like the smart grid.

1 Introduction

Wide-area disturbances have been reported in large-scale power grids. Examples include the 2003 blackouts in North America and Europe [1] and the 2006 system disturbance in Europe [33]. Such disturbances are very costly to modern society and have reminded us of the importance of stable and reliable electricity supply.

Y. Susuki (✉) • T. Hikihara
Department of Electrical Engineering, Kyoto University, Katsura, Nishikyo,
Kyoto 615-8510 Japan
e-mail: susuki@ieee.org; hikihara@kuee.kyoto-u.ac.jp

I. Mezić
Department of Mechanical Engineering, University of California, Santa Barbara,
CA 93106-5070 USA
e-mail: mezic@engineering.ucsb.edu

A. Chakrabortty and M.D. Ilić (eds.), *Control and Optimization Methods for Electric Smart Grids*, Power Electronics and Power Systems 3,
DOI 10.1007/978-1-4614-1605-0_9,

Cascading failure is defined in [14] as a sequence of dependent failures of individual components that successively weakens the power grid. It is regarded as a major cause of disturbance propagation in a system of interconnected power grids. There is a large amount of past and current work on mathematical modeling and numerical simulations of cascading failures as reviewed in [14].

Understanding the dynamics of cascading failure is important for designing the smart grid operation. In [11], the term *Smart Grid* refers to a modernization of the electricity delivery system so it monitors, protects, and automatically optimizes the operation of its interconnected elements, and it will be characterized by a two-way flow of electricity and information to create an automated, widely distributed energy delivery network. This new technology implies the integration of information, communications, and power technologies. It is mainly driven by the large penetration of renewables such as solar and wind power, the aging grid infrastructure (especially in USA), and the emergence of wide-area disturbances as mentioned above. Thus, it is necessary to explore the dynamics of power grids for making the smart grid vision feasible.

In this chapter, we perform numerical analysis of coupled swing dynamics in power grids, based on the notion of power grid instability developed in [28]. In the previous paper, we studied a phenomenon in short-term[1] swing dynamics of multi-machine power grids which we termed the *Coherent Swing Instability* (CSI), based on [9, 10, 19]. This is an emergent and undesirable phenomenon of synchronous machines in a power grid, in which machines in a subset of the grid coherently lose synchronism with the rest of the grid after being subjected to a local disturbance. CSI is a nonlocal instability[2] occurring in a high dimensional dynamical system dominated by inertia in which one nonlinear mode is weak compared with many linear oscillatory modes. It is interpreted as an emergent transmission path of energy from the linear oscillatory modes to the nonlinear mode, which determines the spatially averaged motion of a power grid. The purpose of this chapter is, based on the result on CSI, to describe a dynamical mechanism of cascading failure in a system of interconnected power grids. Here, we use the dynamical systems approach to identify the mechanism: see related work [24, 30, 35].

The contribution of this chapter is a collection of data on CSI and cascading dynamics in a grid configuration of strong inner-connection and weak interconnection. Short-term swing dynamics are mainly studied using the nonlinear swing equations [16], which are a relatively simple dynamical system of ordinary differential equations. By numerical simulations of the swing equations, we analyze the CSI phenomenon in a system of weakly interconnected power grids and exploit the dynamics of CSI to identify the mechanism of cascading failure. The basic test

[1] Zero- to ten-seconds [16].

[2] The phenomenon we study here does not happen upon an infinitesimally small perturbation around an equilibrium of the dynamical system. However, it encompasses the situation when the system escapes a predefined set around the equilibrium. In this way, the notion of instability that we address here is nonlocal.

system used in this chapter is the New England (NE) power grid [3, 23] that we weakly interconnect into a larger power grid. The CSI phenomenon happens for all "unit" NE grids due to a swing wave propagating from other parts of the system and initiates the cascade of unit grid failures. Propagation of swing waves is studied in real power grids (Italy [2], west Japan [31], Texas [21], and Northeast America [5]). Swing dynamics have been reported as a cause of cascading failures in the 2003 blackouts in USA-Canada [34] and Italy [7]. We suggest that a small disturbance in one unit grid grows, spills to the other unit grid as a swing wave, and finally causes the whole system to fail. Throughout, we demonstrate that the CSI could be a part of the dynamical mechanism of cascading failure in power grids. Note that similar data on cascading dynamics in a system of nearly solvable ring power grids is reported in [29].

The rest of this chapter is organized as follows. In Sect. 2, we introduce the phenomenon of CSI using numerical simulations of short-term swing dynamics in the NE power grid. The contents are reported in [28]. In Sect. 3, we provide numerical analysis of a phenomenon of short-term swing dynamics in a system of weakly interconnected NE grids. The system consists of seven "unit" NE grids coupled via weak tie lines in series. In Sect. 4, we discuss topics related to the numerical result and conclude this chapter. Dynamics-based tools for monitoring and control of wide-area disturbances is addressed.

2 Introduction to Coherent Swing Instability

We introduce the phenomenon of CSI using numerical simulations of the NE 39-bus test system. The NE test system or grid is shown in Fig. 1 and is known as a benchmark system exhibiting coupled swing dynamics of synchronous machines [3]. The grid consists of ten generation units (equivalent ten synchronous generators), 39 buses, and lossy AC transmission lines. Most of the buses possess constant active and reactive power loads. The details of the grid, such as unit rating and line data, are available in [23].

2.1 Nonlinear Swing Equations

First of all, we introduce the equations of motion for the NE grid. Assume that generator 1 is the infinite bus[3] in order to explicitly represent the outside of the grid. The short-term swing dynamics of generators 2–10 are modeled by the nonlinear swing equations [16]:

[3] A voltage source of constant voltage and constant frequency.

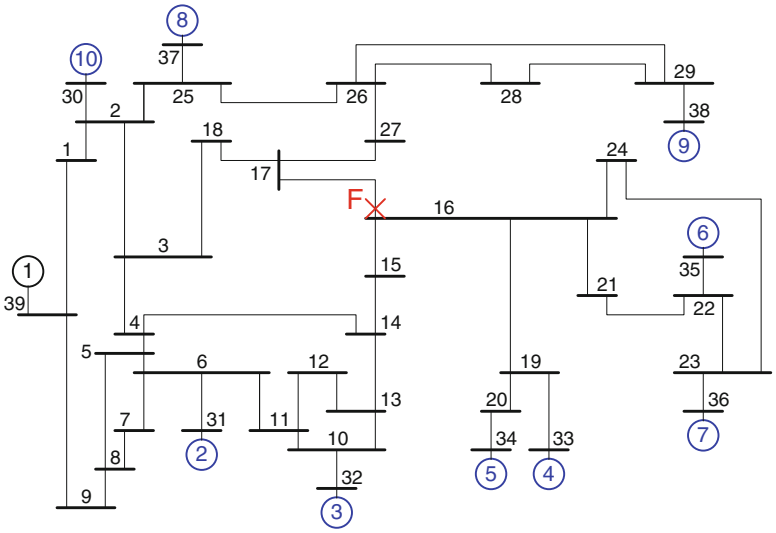

Fig. 1 New England (NE) power grid [3,23]. The grid consists of ten generation units (equivalent ten synchronous generators, which are denoted as circled numbers), 39 buses, and lossy AC transmission lines

$$\left.\begin{aligned} \frac{\mathrm{d}\delta_i}{\mathrm{d}t} &= \omega_i\,, \\ \frac{H_i}{\pi f_\mathrm{b}}\frac{\mathrm{d}\omega_i}{\mathrm{d}t} &= -D_i\omega_i + P_{\mathrm{m}i} \\ &\quad -V_i^2 G_{ii} - \sum_{j=1, j\neq i}^{10} V_i V_j \left\{G_{ij}\cos(\delta_i-\delta_j) + B_{ij}\sin(\delta_i-\delta_j)\right\}, \end{aligned}\right\} \tag{1}$$

where the integer label $i = 2, \ldots, 10$ denotes generator i. The variable δ_i represents the angular position of rotor in generator i with respect to bus 1 and is in radians (rad). The variable ω_i represents the deviation of rotor speed in generator i relative to system angular frequency $2\pi f_\mathrm{b} = 2\pi \times (60\,\mathrm{Hz})$ and is in radians per second (rad/s). We set the variable δ_1 to a constant, because bus 1 is assumed to be the infinite bus. The parameters f_b, H_i, D_i, $P_{\mathrm{m}i}$, V_i, G_{ii}, G_{ij}, and B_{ij} are in per unit system except for f_b in Hertz (Hz) and for H_i and D_i in seconds (s). The mechanical input power $P_{\mathrm{m}i}$ to generator i and the internal voltage V_i of generator i are normally assumed to be constant for short-term swing dynamics [16]. The parameter H_i denotes the per unit time inertia constant of generator i, and D_i denotes its damping coefficient. The parameter G_{ii} denotes the internal conductance, and $G_{ij} + \mathrm{i}B_{ij}$ (where i is the imaginary unit) denotes the transfer admittance between generators i and j. They are the parameters that change as the network topology changes. Electrical loads are modeled as passive admittances.

2.2 Numerical Simulations

We numerically simulate coupled swing dynamics of generators 2–10. All numerical simulations discussed in this chapter were performed using MATLAB: for example, the function `ode45` was used for numerical integrations of (1). The voltage V_i and the initial condition $(\delta_i(0), \omega_i(0) = 0)$ for generator i are fixed using power flow computation. The inertia constant H_i is the same as in [23]. For the simulation, we use the following load condition: $P_{\mathrm{m}i}$ and constant power loads are 50% at their rating. The damping D_i is fixed at 0.005 s for each generator.[4] The elements G_{ii}, G_{ij}, and B_{ij} are calculated using the data in [23] and the result on power flow computation. Also, we use the following fault condition: each generator operates at a steady condition at $t = 0$ s. Then a three-phase fault happens at point F near bus 16 at $t = 1\,\mathrm{s} - 20/(60\,\mathrm{Hz}) = 2/3\,\mathrm{s} \approx 0.67\,\mathrm{s}$, and line 16–17 trips at $t = 1$ s. The fault duration is 20 cycles of a 60 Hz sinusoidal wave. The fault is modeled by adding a small impedance (10^{-7}i) between bus 16 and the ground.

Figure 2 shows the time responses of angular position δ_i and relative rotor speed ω_i of generator i. Before $t \approx 0.67$ s (this is the onset time of fault), each generator operates at a steady condition. In the fault duration from $t \approx 0.67$ to 1 s, all the generators 2–10 accelerate from their steady conditions. After the line trip at $t = 1$ s, they respond in an oscillatory manner. These oscillations are bounded during the period from $t = 1$ to 8 s. At about time 8 s, they begin to grow coherently and finally diverge. That is, every generator loses synchronism with the infinite bus at the same time. This corresponds to the growth of amplitude of inter-area mode oscillation between the NE grid and the infinite bus, namely, the outside of the grid. This is typical of the CSI phenomenon.

In the following, we demonstrate two methods for elucidating dynamical features of the phenomenon. First, we use the notion of *collective* variables for characterizing the spatially averaged motion of a power grid. The collective variables are well known as the COA (Center-Of-Angle) variables [3]. For the NE grid, the COA δ_{COA} and its time derivative ω_{COA} are defined as

$$\delta_{\mathrm{COA}} := \sum_{i=2}^{10} \frac{H_i}{H}\delta_i, \quad \omega_{\mathrm{COA}} := \frac{\mathrm{d}\delta_{\mathrm{COA}}}{\mathrm{d}t} = \sum_{i=2}^{10} \frac{H_i}{H}\omega_i, \tag{2}$$

where $H := \sum_{i=2}^{10} H_i$. The variables $(\delta_{\mathrm{COA}}, \omega_{\mathrm{COA}})$ describe the averaged motion of all the generators in the grid. Figure 3 plots the trajectory of (1) showing the CSI phenomenon in Fig. 2 on δ_{COA}–ω_{COA} plane. The trajectory starts near the origin at time 0 s, makes a couple of almost periodic loops around the initial point, and finally diverges.

[4] In the case that the relative rotor speed ω_i is in per unit system with base quantity $2\pi f_{\mathrm{b}}$, the damping coefficient $D_i = 0.005$ s is equal to 1.88 in per unit system with its base quantity $1/(2\pi f_{\mathrm{b}})$.

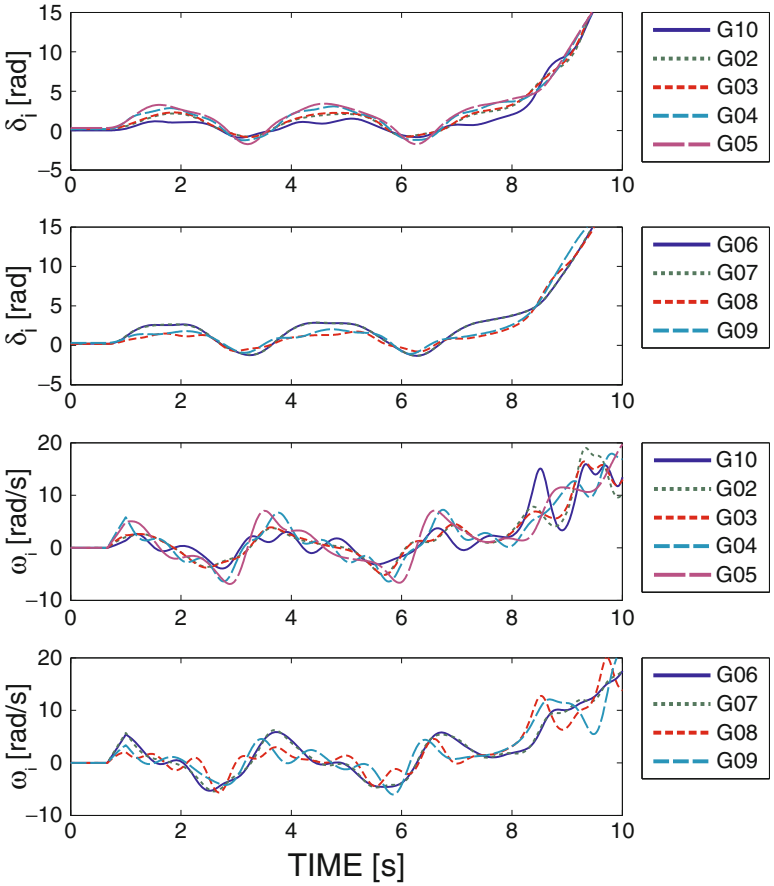

Fig. 2 Coupled swing dynamics in the NE power grid. The upper two plots are for angular positions δ_i of the nine generators, and the lower plots are for the relative rotor speed ω_i

Second, we use the *Proper Orthonormal Decomposition* (POD) in order to decompose the phenomenon in Fig. 2, which has been used in the context of power system analysis [17, 24]. POD provides a basis for the modal decomposition of an ensemble of functions, such as data obtained in the course of experiments, and provides energy-wise, the most efficient way of capturing the dominant components of the process [12, 13]. Consider finite simulation outputs of angular positions, $\{\delta_i(nT_\mathrm{s})\}$ $(i = 2, \ldots, 10, n = 0, \ldots, N_\mathrm{s} - 1)$, where T_s is the sampling period of outputs, and N_s is the number of samples. The outputs are represented by

$$\delta_i(nT_\mathrm{s}) = \sum_{j=1}^{9} e_{ij} a_j(nT_\mathrm{s}). \tag{3}$$

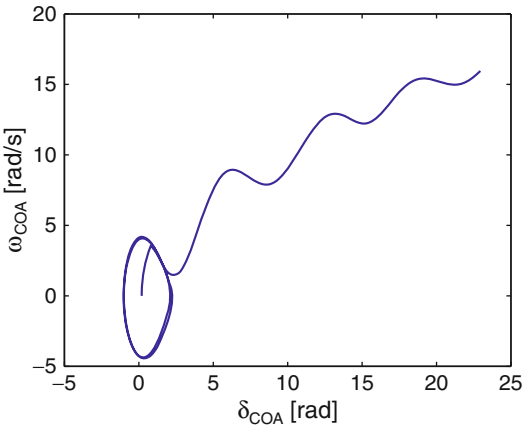

Fig. 3 Collective dynamics in the NE 39-bus test system. This plot corresponds to the projected trajectory onto the plane of the Center-Of-Angle (COA) variables $(\delta_{\mathrm{COA}}, \omega_{\mathrm{COA}})$ for the phenomenon observed in Fig. 2

We require the time-invariant basis vectors $\{e_{ij}\}$ $(i = 2, \ldots, 10)$ to be orthonormal and closest in energy norm to the output, and call them the *Proper Orthonormal Modes* (POMs). Every vector $\{e_{ij}\}$ is obtained by computing the correlation matrix R from $\{\delta_i(nT_\mathrm{s})\}$ and by finding the orthonormal eigenvectors of R: see [12] for details. The time-varying coefficient a_j $(j = 1, \ldots, 9)$ in the POD holds the following correlation property: $\langle a_j a_k \rangle = \langle a_j^2 \rangle$ (if $j = k$) or 0 (otherwise), where $\langle \bullet \rangle$ represents a time average of $\{\bullet\}$. POMs are ordered by $\langle a_j^2 \rangle \geq \langle a_{j+1}^2 \rangle$.

POMs are obtained using $N_\mathrm{s} = 5341$ snapshots in the simulation outputs partially shown in Fig. 2. The time interval is [1 s, 90 s], and T_s is equal to 1/(60 Hz). Figure 4 shows the projection of the trajectory of (1) onto subspaces spanned by every POM. The projected trajectory $(a_j(nT_\mathrm{s}), b_j(nT_\mathrm{s}))$ for the j-th POM $(j = 1, \ldots, 9)$ is computed as

$$a_j(nT_\mathrm{s}) = \sum_{i=2}^{10} e_{ij}\,\delta_i(nT_\mathrm{s}), \quad b_j(nT_\mathrm{s}) = \sum_{i=2}^{10} e_{ij}\,\omega_i(nT_\mathrm{s}), \tag{4}$$

where $n = 0, \ldots, N_\mathrm{s} - 1$ (because of the smallness of the damping term we use the same modes for the angles and their time derivatives). In the first POM, the trajectory shows a transition from periodic motion to divergent one. The trajectory of the first POM coincides with the trajectory projected onto the COA plane in Fig. 3 by rotating it by 180° around the origin. On the other hand, in the other POMs, each trajectory shows a periodic or quasi-periodic motion. This is confirmed by looking at the results on power spectra (see [28]). The emergent phenomenon shown in Fig. 2 happens in the dynamical system with one *nonlinear* mode and many linear oscillatory modes.

These results enable us to explain the CSI phenomenon. In the dynamical system, the linear oscillator modes are strong because the interconnection term in (1) is strong (see [28]) due to the structure of interaction between generators, where

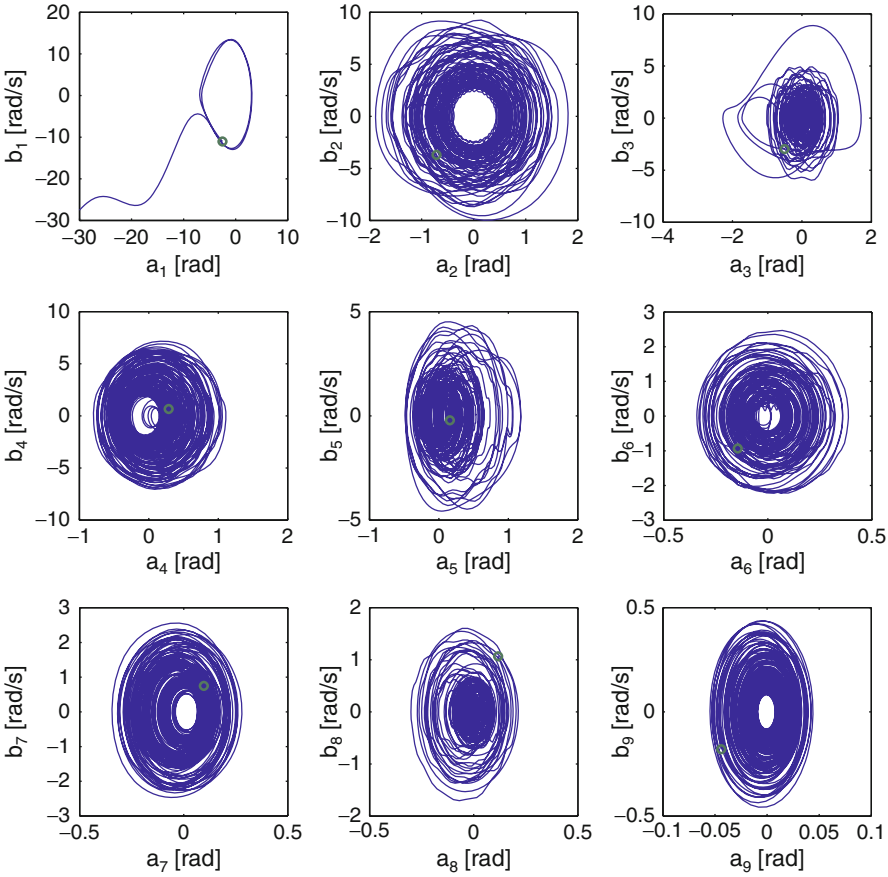

Fig. 4 Projected trajectories onto Proper Orthonormal Mode (POM) planes of the time series of coefficients a_j during [1 s, 90 s] with sampling frequency 60 Hz

many generators affect the dynamics of any single one. Compared with the linear modes, because the local term in (1), which represents the interaction between any generator and the infinite bus, is weak, the nonlinear mode is also weak. The linear oscillations then act as perturbations on the nonlinear mode. The perturbations are normally small due to the weakness of the coupling between the modes, but they become large if any linear mode and the nonlinear one satisfy a condition of internal resonance (see [10]). In this way, the amplitude of the first nonlinear POM in Fig. 4, or equivalently the projected COA trajectory in Fig. 3 can escape the region of bounded motions in the dynamical system of the first POM. This is the dynamical mechanism causing the CSI. It implies that the coupling of grid architecture and dynamics of the system matters the most.

Note that the NE grid is a test benchmark system, being a slight simplification of the real NE grid. Although the mathematical models are derived under reasonable assumptions for short-term rotor swing stability, they do not necessarily represent the true dynamics of the NE grid. Here, it is valuable to discuss whether the CSI in Fig. 2 can occur in a real power grid. The fault duration, which we set at 20 cycles in the simulation, is normally less than ten cycles. Such a long duration may imply the malfunction of protection systems, and hence the CSI in Fig. 2 may be regarded as a rare event in short-term swing dynamics. However, in Sect. 3 we will show that in a system of interconnected power grids, CSI is observed in the case of fault duration eight cycles. Furthermore, in the simulation we ignore the effect of load dynamics. The effect is normally negligible because it does not affect short-term swing dynamics [16] and will not cause any drastic change of simulation results. Thus, we suggest that CSI is a phenomenon that can occur for various configurations close to real power grids.

3 Dynamical Mechanism of Cascading Failures

In this section, we study a phenomenon of short-term swing dynamics in a system of Weakly Interconnected NE (WINE) grids. The system is shown in Fig. 5 and consists of the $N(=7)$ NE grids (each of which we call the unit grid), the infinite bus, and weak interconnections. Each unit grid in Fig. 5 has equal specification of synchronous generators, loads, ac transmission lines, and network topology. The N unit grids are joined to each other in series via weak interconnections. Bus 24 in unit grid #i ($i = 1, \ldots, N-1$) and bus 39 in unit grid #$(i+1)$ are joined by a transmission line. We make the three assumptions: (i) generator 1 in unit grid #1 is the infinite bus; (ii) there is no generator 1 in the other unit grids; and (iii) the impedance of lines joining two different unit grids is three times as large as those of line joining buses 26 and 29. The reason why we chose line 26–29 is that it has the largest value of impedance in each unit grid. Thus, we *weakly* interconnect the seven unit grids, in each of these unit grids, nine synchronous machines are *strongly* connected.

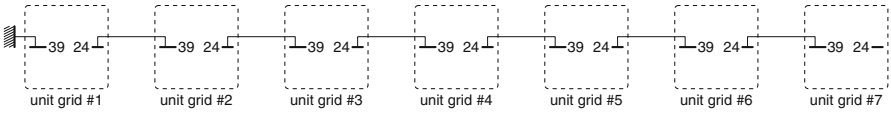

Fig. 5 System of Weakly Interconnected New England (WINE) grids. The system consists of the $N(=7)$ NE power grids and weak tie lines joining them. Generator 1 in unit grid #1 is assumed to be the infinite bus

3.1 Nonlinear Swing Equations

In the same manner as the single NE grid in Sect. 2, we use the nonlinear swing equations for modeling and analysis of coupled swing dynamics in the WINE system. The short-term swing dynamics of generator j in unit grid #i ($j = 2, \ldots, 10, i = 1, \ldots, N$) are represented by

$$\left.\begin{aligned} \frac{\mathrm{d}\delta_{ij}}{\mathrm{d}t} &= \omega_{ij}\,, \\ \frac{H_j}{\pi f_\mathrm{b}}\frac{\mathrm{d}\omega_{ij}}{\mathrm{d}t} &= P_{\mathrm{m}\,ij} - D_j\omega_{ij} \\ &\quad -V_{ij}V_{11}\{G_{ij,11}\cos(\delta_{ij}-\delta_{11}) + B_{ij,11}\sin(\delta_{ij}-\delta_{11})\} \\ &\quad -V_{ij}^2 G_{ij} - \sum_{k=1,k\neq i}^{N}\sum_{l=2,l\neq j}^{10} V_{ij}V_{kl}\{G_{ij,kl}\cos(\delta_{ij}-\delta_{kl}) \\ &\quad +B_{ij,kl}\sin(\delta_{ij}-\delta_{kl})\}. \end{aligned}\right\} \tag{5}$$

The variable δ_{ij} represents the angular position of rotor in generator j in unit grid #i with respect to the infinite bus and is in radians (rad). The variable ω_{ij} represents the deviation of rotor speed in generator i relative to system angular frequency $2\pi f_\mathrm{b}$ and is in radians per second (rad/s). The variable δ_{11} is the angular position of the infinite bus and becomes constant from its definition. The parameters H_j, $P_{\mathrm{m}\,ij}$, D_j, V_{ij}, $G_{ij,ij}$, and $G_{ij,kl}+\mathrm{i}B_{ij,kl}$ are in per unit system except for H_j and D_j in seconds (s). The constants H_j and D_j are introduced in Sect. 2.1. The constant $P_{\mathrm{m}\,ij}$ is the mechanical input power to generator j in unit grid #i, and V_{ij} is the internal voltage of generator j in unit grid #i. They are assumed to be constant in the same manner as in Sect. 2. The constant $G_{ij,ij}$ denotes the internal conductance of generator j in unit grid #i, and $G_{ij,kl}+\mathrm{i}B_{ij,kl}$ denotes the transfer admittance between generators j in unit grid #i and l in unit grid #k. The constant V_{11} is the voltage of the infinite bus, and $G_{ij,11}+\mathrm{i}B_{ij,11}$ is the transfer admittance between generator j in unit grid #i and the infinite bus. The admittance $G_{ij,kl}+\mathrm{i}B_{ij,kl}$ is the parameters that change as the network topology changes.

3.2 Numerical Simulations

We numerically simulate coupled swing dynamics of 63 generators. Basically, the system parameters are based on the data provided in [23] and in Sect. 2. The voltages V_{ij} and initial conditions $(\delta_{ij}(0), \omega_{ij}(0)) = (\delta_{ij}^*, 0\,\mathrm{rad/s})$ are fixed using power flow computation. The constant δ_{ij}^* is the value of angular position δ_{ij} at a steady operating condition before the fault. The parameter H_j is the same as in Sect. 2. The mechanical input power $P_{\mathrm{m}\,ij}$ and constant power loads are also the same as in [23].

The damping D_i is fixed at 0.01 s for each generator. The elements $G_{ij,ij}$, $G_{ij,kl}$, and $B_{ij,kl}$ are calculated using the data in [23]. We use the following fault condition: each generator operates at the steady condition at $t < 1\,\mathrm{s} - 8/(60\,\mathrm{Hz}) \approx 0.87\,\mathrm{s}$, a three-phase fault happens near bus 39 in unit grid #1 at $t \approx 0.87\,\mathrm{s}$, and line 1–39 trips at $t = 1\,\mathrm{s}$. The fault duration is eight cycles of a 60 Hz sinusoidal wave. The fault is simulated by adding a small impedance (10^{-7}i) between bus 39 in unit grid #1 and the ground.

Figure 6 shows the time responses of angular positions δ_{ij}. The notation #i–Gj in the figure indicates that the corresponding colored line shows the time response of δ_{ij} for generator j in unit grid #i. The local fault happens in unit grid #1. The angular positions in unit grid #1 show swings at the onset time of fault $t \approx 0.87\,\mathrm{s}$. On the other hand, the angular positions in unit grids #2 to #7 do not show any swings at the onset time and do remain at their steady conditions. After a while, the swings in unit grid #1 propagate through the WINE system and reach the last unit grid #7 at about time $t = 4\,\mathrm{s}$. This propagation causes secondary swings in every unit grid. After reaching the last unit grid, it propagates through the grid in the backwards direction. During this initial swing propagation, the angular positions in each unit grid show coherent oscillations similar to that of the single NE grid in Sect. 2. The oscillations in unit grid #1 are damped due to both nonzero damping and dispersion effect caused by weak interconnections. The oscillations in the other unit grids are also damped and then show slight growth as time passes. Although the slight growth of angular positions is undesirable, it is still bounded and does not represent the loss of transient stability of synchronous generators in these unit grids. When the swings return to unit grid #1 at time $t = 9\,\mathrm{s}$, the angular positions δ_{1j} begin to grow in a coherent manner and finally diverge. After the first divergence, the angular positions δ_{2j} in unit grid #2 next begin to diverge in a coherent manner. This cascade of coherent divergences continues up to the last unit grid. The coherent divergence in a unit grid corresponds to the loss of transient stability. This result indicates that a local disturbance in one unit grid grows, spills to the other grids, and finally causes the whole system to fail.

In the single NE grid, the motion of a hidden nonlinear mode was captured by projecting the full-system dynamics onto the phase plane of COA variables. Since the POD approach leads to the same nonlinear mode as the COA approach, we now investigate the cascade of unit grid failures using the notion of COA. Here, it is not effective to define the COA for the full-system dynamics of 63 generators, because it does not provide any insight of the interaction of different unit grids. In this case, we define the COA for each unit grid i ($i = 1, \ldots, N$) as

$$\delta_{i\,(\mathrm{COA})} := \sum_{j=2}^{10} \frac{H_j}{H} \delta_{ij}, \quad \omega_{i\,(\mathrm{COA})} := \sum_{j=2}^{10} \frac{H_j}{H} \omega_{ij}, \tag{6}$$

where $\delta_{i\,(\mathrm{COA})}$ denotes the COA of unit grid #i and $\omega_{i\,(\mathrm{COA})}$ its time derivative. The variables represent the spatially averaged motion of all the generators in unit grid #i. Figure 7 plots the trajectory of (5) showing the cascade in Fig. 6 on

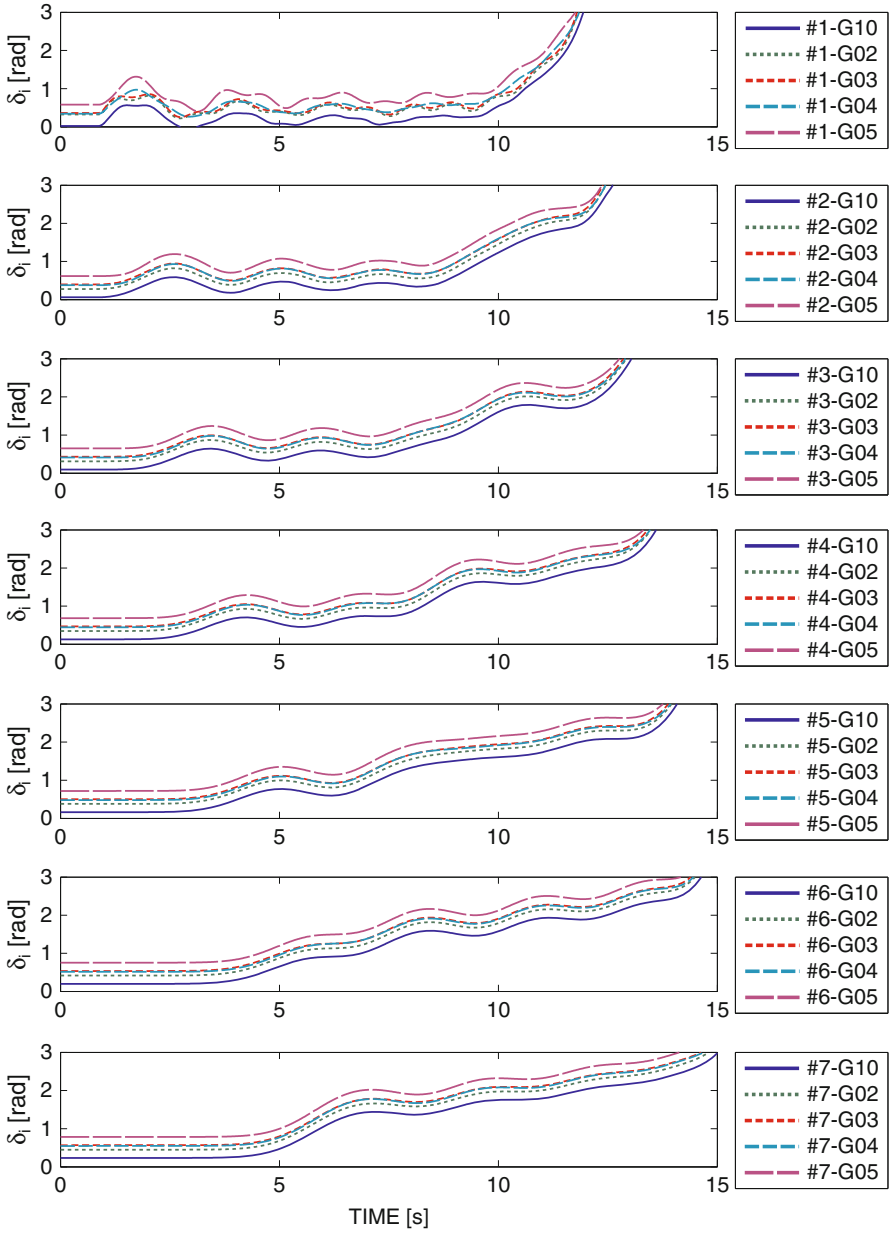

Fig. 6 Coupled swing dynamics in a system of WINE grids. The notation #i–Gj denotes the time response of angular position δ_{ij} of generator j in unit grid #i

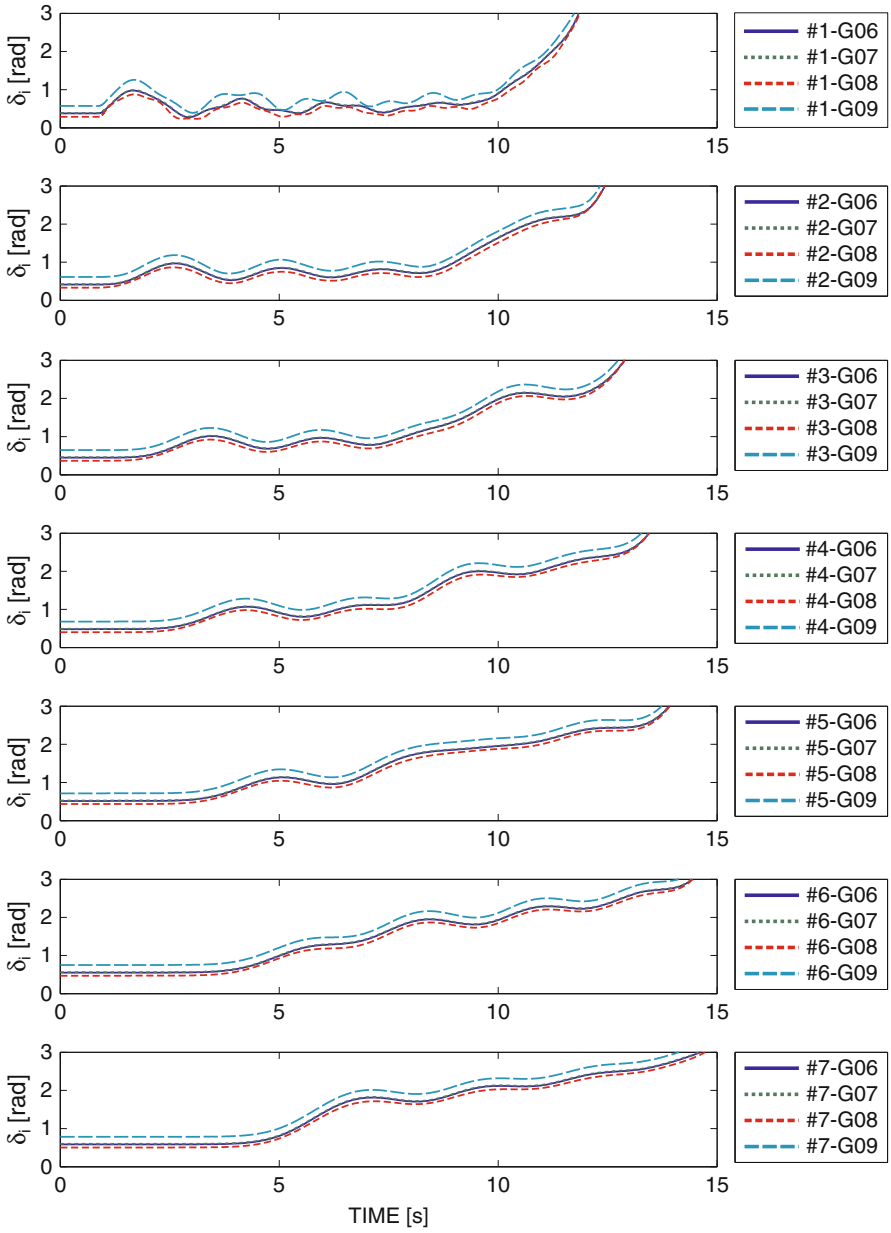

Fig. 6 (continued)

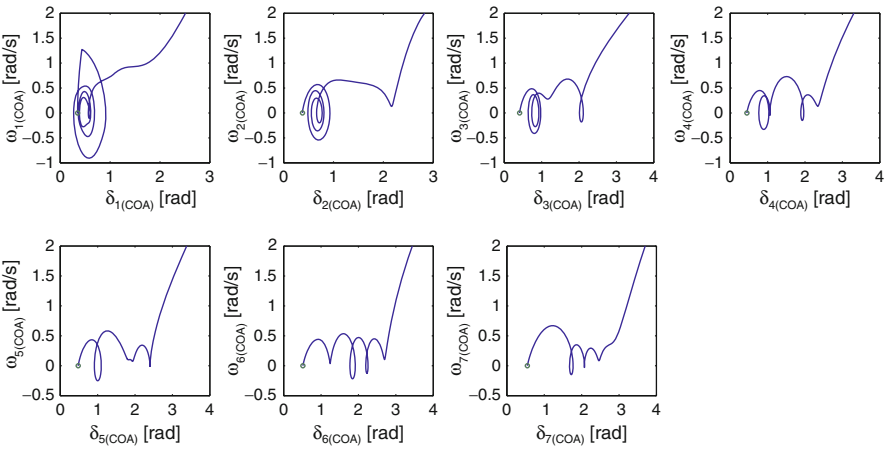

Fig. 7 Collective dynamics in a system of WINE grids. These plots correspond to the projected trajectories onto the planes of the COA variables (6) for the phenomenon shown in Fig. 6

$\delta_{i\,(\mathrm{COA})}$–$\omega_{i\,(\mathrm{COA})}$ planes. In unit grid #1, the trajectory executes damped oscillations for a while. However, the swings which return to unit grid #1 interrupt the trajectory and *kick* it. This kicking induces the divergence of trajectory in unit grid #1. In unit grid #2, the trajectory is kicked twice and finally diverges. The first kick is due to the swings propagating from unit grid #3, and the second kick is due to the divergence of unit grid #1. Similar behaviors for the trajectories of unit grids #3 and #4 are identified in Fig. 7. On the other hand, the trajectories of unit grids #5 to #7 show different behaviors. They do not show clear periodic motions and do drift to right when the swings kick them twice, and finally they diverge.

4 Summary and Discussion

In this chapter, we have studied the emergent instability phenomenon, termed the CSI, in power grids. Section 3 was devoted to numerical analysis of coupled swing dynamics in the WINE system shown in Fig. 5. The analysis suggests that the CSI phenomenon happens for all of the unit grids due to a swing wave propagating from other parts of the system and initiates the cascade of unit grid failures. In this section, we discuss several topics related to the result and close this chapter.

The analysis in Sect. 3 was performed by introducing the COA variables for each unit grid with coherent generators. The COA variables were useful for the dynamical analysis performed in this chapter, because the WINE system possessed a trivial set of strongly inner-connected grids, in each of which generators may exhibit coherent motions. Generally speaking, it is not easy to find such a set of coherent generators for real power grids. Identifying coherent generators is necessary for

applying the developed theory to data on cascading failures in real power grids. Such identification techniques have been reported by many researchers, for example, the Lyapunov function method [22], the singular perturbation method [4, 6, 36], and the Koopman mode analysis (KMA) [27] that is introduced in the last of this section. These methods can identify a set of unit grids consisting of coherent generators, so that one can investigate the COA dynamics for each identified grid.

As introduced in Sect. 1, cascading failures are fairly complicated phenomena emerging in interconnected dynamical systems. It would be impossible to obtain a simple mechanism that can explain all dynamics and events in a cascading failure. For a power grid consisting of many sub-grids, the instability shown in Sect. 2 describes a failure of one sub-grid caused by the loss of transient stability. In this chapter, we show that a sequence of sub-grid failures is induced by a sequence of CSIs. Thus, we suggest that the CSI could be a part of the dynamical mechanism of cascading failure of large-scale power grids.

Also, it is often said that causes of cascading failures include correct/incorrect relay operations and hidden failures [32] that are discontinuous actions in the dynamics of power grids. This is naturally modeled by a hybrid dynamical system. In [30], the authors use a hybrid dynamical system for modeling and analysis of the cascading failure leading to the 2003 blackout in Italy. Analysis of the hybrid model shows that the swing dynamics, especially desynchronization of individual generators, result from a network switching with a simple relay feedback controller. On the other hand, in this chapter we describe another scenario of swing dynamics leading to desynchronization of individual generators *without* any network switching. This is a counterexample to the standard argument as stated in the beginning of this paragraph. Of course, the dynamic phenomenon that we studied in this chapter may be an extreme example for cascading failures. Our mechanism of cascading failure will need further research in more realistic test systems and for practical data on cascading failures.

It was suggested that cascading failures are partly due to the loss of transient stability based on real data, for example, the September 2003 blackout in Italy [7]. Our study suggests that such instability could happen via a swing wave propagation mechanism. To the best of our knowledge, there is yet no real data proving that the swing wave propagation is an initiation of cascading failure. In order to identify our mechanism in real power grids, a measurement system that can simultaneously monitor global dynamics of large-scale power grids is needed. This can be carried out with the emerging technology of wide-area measurement with the aid of synchronized PMUs[5] (see e.g. [8, 25]).

The cascading dynamics that we studied in Sect. 3 are, needless to say, an undesirable phenomenon of power grids and should be prevented by grid design or avoided by control. Figure 6 shows that the difference of COAs increases as time passes. This large difference may trigger the action of protection systems that are normally equipped with a tie line. A key point for control is how to detect the

[5]Phasor Measurement Units.

propagation of swing waves in a power grid. One possible solution is again the emerging wide-area measurement-based control and analysis (see e.g. [15]). Wide-area measurement is expected to stabilize spatiotemporal dynamics in large-scale power grids.

In the current analysis, we used the dynamical systems approach to elucidate a core cause of wide-area disturbances. As a next step, it is necessary to consider how to apply the dynamical perspective to monitoring and control of power grids. Currently, we are developing methodology and tools for monitoring of power grids based on the result. A key method in our development is the Koopman mode analysis (KMA) that is based on a fully nonlinear spectral theory and represents an extension of linear oscillatory mode analysis [18]. KMA is dynamically consistent with underlying (possibly nonlinear) physics and provides a new approach to model validation and reduction [18, 20]. We show that KMA provides a method for identifying coherent generators from sensor data [27] and defines a *precursor* to CSI with its computation method based on sensor data and mathematical modeling [26]. The precursor is based on the discovery of emergent transmission path of energy from many linear oscillatory modes to the nonlinear mode as mentioned in Sect. 2. Both the methods need data collected in a real power grid and computation based on a mathematical model. Hence, they would be suitable as tools implemented to the future smart grid in which the physical power network is overlaid with an information network.

Acknowledgments We are grateful to Professor Petar Kokotović and Professor Joe H. Chow for discussions and valuable suggestions. This work was supported in part by JSPS Postdoctoral Fellowships for Research Abroad, in part Grant-in-Aid for Global COE Program "Education and Research on Photonics and Electronics Science and Engineering," MEXT, Japan, and in part NICT Project ICE-IT (Integrated Technology of Information, Communications, and Energy). During this work, Y. Susuki was with the Department of Mechanical Engineering at the University of California, Santa Barbara.

References

1. Andersson G, Donalek P, Farmer R, Hatziargyriou N, Kamwa I, Kundur P, Martins N, Paserba J, Pourbeik P, Sanchez-Gasca J, Schulz R, Stankovic A, Taylor C, Vittal V (2005) Causes of the 2003 major grid blackouts in North America and Europe, and recommended means to improve system dynamic performance. IEEE Trans Power Syst 20(4):1922–1928
2. Arcidiacono V, Ferrari E, Saccomanno F (1976) Studies on damping of electromechanical oscillations in multimachine systems with longitudinal structure. IEEE Trans Power App Syst PAS-95(2):450–460
3. Athay T, Podmore R, Virmani S (1979) A practical method for the direct analysis of transient stability. IEEE Trans Power App Syst PAS-98(2):573–584
4. Avramović B, Kokotović PV, Winkelman JR, Chow JH (1980) Area decomposition for electromechanical models of power systems. Automatica 16:637–648
5. Chow JH (2010) Personal communication
6. Chow JH, Cullum J, Willoughby A (1984) A sparsity-based technique for identifying slow-coherent areas in large power systems. IEEE Trans Power App Syst PAS-103(3):463–473

7. Corsi S, Sabelli C (2004) General blackout in Italy Sunday September 28, 2003, h. 03:28:00. In: Proceedings of IEEE PES general meeting, Denver, USA, vol 2, pp 1691–1702
8. De La Ree J, Centeno V, Thorp JS, Phadke AG (2010) Synchronized phasor measurement applications in power systems. IEEE Trans Smart Grid 1(1):20–27
9. Du Toit P, Mezić I, Marsden J (2009) Coupled oscillator models with no scale separation. Physica D 238(5):490–501
10. Eisenhower B, Mezić I (2010) Targeted activation in deterministic and stochastic systems. Phys Rev E 81:026,603
11. Electric Power Research Institute (2009) Report to NIST on the Smart Grid Interoperability Standards Roadmap (Contract No. SB1341-09-CN-0031), June 17, 2009
12. Feeny BF, Kappagantu B (1998) On the physical interpretation of proper orthogonal modes in vibrations. J Sound Vib 211(4):607–616
13. Holmes P, Lumley JL, Berkooz G (1996) Turbulence, coherent structures, dynamical systems, and symmetry. Cambridge University Press, Cambridge
14. IEEE PES CAMS Task Force on Cascading Failure (2008) Initial review of methods for cascading failure analysis in electric power transmission. In: Proceedings of IEEE PES general meeting, Pittsburgh
15. Kamwa I, Grondin R, Hébert Y (2001) Wide-area measurement based stabilizing control of large power systems—A decentralized/hierarchical approach. IEEE Trans Power Syst 16(1):136–153
16. Kundur P (1994) Power system stability and control. McGraw-Hill, New York
17. Messina AR, Vittal V (2007) Extraction of dynamic patterns from wide-area measurements using empirical orthogonal functions. IEEE Trans Power Syst 22(2):682–692
18. Mezić I (2005) Spectral properties of dynamical systems, model reduction and decompositions. Nonlinear Dyn 41:309–325
19. Mezić I (2006) On the dynamics of molecular conformation. Proc Natl Acad Sci USA 103(20):7542–7547
20. Mezić I, Banaszuk A (2004) Comparison of systems with complex behavior. Physica D 197:101–133
21. Murphy RJ (1996) Disturbance recorders trigger detection and protection. IEEE Comput Appl Power 9(1):24–28
22. Ohsawa Y, Hayashi M (1981) Construction of power system transient stability equivalents using the Lyapunov function. Int J Electron 50(4):273–288
23. Pai MA (1989) Energy function analysis for power system stability. Kluwer Academic Publishers, Boston
24. Parrilo PA, Lall S, Paganini F, Verghese GC, Lesieutre BC, Marsden JE (1999) Model reduction for analysis of cascading failures in power systems. In: Proceedings of American Control Conference, San Diego, pp 4208–4212
25. Phadke AG (1993) Synchronized phasor measurement in power systems. IEEE Comput Appl Power 6(2):10–15
26. Susuki Y, Mezić I (2011) Nonlinear Koopman modes and a precursor to power system swing instabilities. IEEE Trans Power Syst (submitted for possible publication)
27. Susuki Y, Mezić I (2011) Nonlinear Koopman modes and coherency identification of coupled swing dynamics. IEEE Trans Power Syst 26(4):1894–1904
28. Susuki Y, Mezić I, Hikihara T (2011) Coherent swing instability of power grids. J Nonlinear Sci 21(3):403–439
29. Susuki Y, Mezić I, Hikihara T (2010) Coherent swing instability of power systems and cascading failures. In: Proceedings of IEEE PES general meeting, Minneapolis
30. Susuki Y, Takatsuji Y, Hikihara T (2009) Hybrid model for cascading outage in a power system: A numerical study. IEICE Trans Fund Electr E92-A(3):871–879
31. Tamura Y (1995) Possibility of parametric resonance in power system. Trans Electr Eng Jpn 112-B(8):657–663 (in Japanese)
32. Thorp JS, Phadke AG, Horowitz SH, Tamronglak S (1998) Anatomy of power system disturbance: importance sampling. Int J Electr Power 20(2):147–152

33. Union for the Coordination of the Transmission of Electricity (2007) Final Report on System Disturbance on 4 November 2006, January 2007
34. U.S.-Canada Power System Outage Task Force (2004) Final Report on the August 14, 2003, Blackout in the United States and Canada: causes and recommendations, April 2004
35. Venkatasubramanian VM, Li Y (2004) Analysis of 1996 Western American electric blackouts. In: Proceedings of Bulk Power System Dynamics and Control—VI, Cortina d'Ampezzo, Italy, pp 685–721
36. Winkelman JR, Chow JH, Bowler BC, Avramović B, Kokotović PV (1981) An analysis of interarea dynamics of multi-machine systems. IEEE Trans Power App Syst PAS-100(2): 754–763